Asian Journal of Pharmaceutical Sciences 19 (2024) 100928

Available online at www.sciencedirect.com

ScienceDirect

journal homepage: www.elsevier.com/locate/AJPS

Research Article

Advancing ophthalmic delivery of flurbiprofen via synergistic chiral resolution and ion-pairing strategies

Zhining Ma[a,1], *Yuequan Wang*[b,1], *Huiyang He*[b], *Tong Liu*[c], *Qikun Jiang*[b,*], *Xiaohong Hou*[d,*]

[a] *School of Pharmacy, Shenyang Pharmaceutical University, Shenyang 110016, China*
[b] *Wuya College of Innovation, Shenyang Pharmaceutical University, Shenyang 110016, China*
[c] *Liaoning Provincial Institute of Drug Inspection and Testing, Shenyang 110036, China*
[d] *School of Pharmaceutical Engineering, Shenyang Pharmaceutical University, Shenyang 110016, China*

ARTICLE INFO

Article history:
Received 8 October 2023
Revised 24 December 2023
Accepted 16 January 2024
Available online 22 May 2024

Keywords:
Flurbiprofen
Anti-inflammatory
Ophthalmic delivery
Chiral resolution
Ion-pairing

ABSTRACT

Flurbiprofen (FB), a nonsteroidal anti-inflammatory drug, is widely employed in treating ocular inflammation owing to its remarkable anti-inflammatory effects. However, the racemic nature of its commercially available formulation (Ocufen®) limits the full potential of its therapeutic activity, as the (*S*)-enantiomer is responsible for the desired anti-inflammatory effects. Additionally, the limited corneal permeability of FB significantly restricts its bioavailability. In this study, we successfully separated the chiral isomers of FB to obtain the highly active (*S*)-FB. Subsequently, utilizing ion-pairing technology, we coupled (*S*)-FB with various counter-ions, such as sodium, diethylamine, trimethamine (TMA), and l-arginine, to enhance its ocular bioavailability. A comprehensive evaluation encompassed balanced solubility, octanol-water partition coefficient, corneal permeability, ocular pharmacokinetics, tissue distribution, and *in vivo* ocular anti-inflammatory activity of each chiral isomer salt. Among the various formulations, S-FBTMA exhibited superior water solubility (about 1–12 mg/ml), lipid solubility ($1 < \lg P_{ow} < 3$) and corneal permeability. In comparison to Ocufen®, S-FBTMA demonstrated significantly higher *in vivo* anti-inflammatory activity and lower ocular irritability (such as conjunctival congestion and tingling). The findings from this research highlight the potential of chiral separation and ion-pair enhanced permeation techniques in providing pharmaceutical enterprises focused on drug development with a valuable avenue for improving therapeutic outcomes.

* Corresponding authors.
E-mail addresses: jiangqikunlqq@163.com (Q. Jiang), syphu_houxiaohong@163.com (X. Hou).
[1] These authors contributed equally to this work.
Peer review under responsibility of Shenyang Pharmaceutical University.

https://doi.org/10.1016/j.ajps.2024.100928

1. Introduction

In recent years, there has been a noticeable increase in the prevalence of ocular inflammation, stemming from various causes such as eye irritation [1,2], allergies, infections, and surgical procedures. Effectively treating ocular inflammation requires the selection of appropriate medications based on the underlying etiology [3,4]. Nonsteroidal anti-inflammatory drugs (NSAIDs) have emerged as the predominant class of ophthalmic anti-inflammatory agents due to their anti-inflammatory and analgesic properties. Currently, NSAIDs constitute approximately 75% of the market for anti-inflammatory drugs in ophthalmology [5]. One of the key advantages of NSAIDs lies in their ability to mitigate inflammation without inducing adverse effects such as elevated intraocular pressure, secondary infections, or steroid hormone-induced cataracts [6]. Their favorable safety profile and efficacy have positioned NSAIDs as a preferred therapeutic choice in managing ocular inflammation, contributing significantly to their dominance in the ophthalmic anti-inflammatory market [7,8].

Flurbiprofen sodium (FBNa) eyedrop (Ocufen®) stands as a widely employed commercial NSAID in the field of ophthalmology [9]. Flurbiprofen (FB) manifests in two chiral isomers, namely (*S*)-(+)-flurbiprofen and (*R*)-(-)-flurbiprofen. Despite their identical chemical structures, their three-dimensional configurations differ, giving rise to potential disparities in their pharmacological properties, including pharmacodynamics, metabolic pathways, and side effect profiles [10,11]. Studies have demonstrated that (*S*)-flurbiprofen (S-FB) exhibits superior anti-inflammatory activity compared to (*R*)-flurbiprofen (R-FB), with the former displaying a 100-fold stronger inhibitory effect on cyclooxygenase-1 (COX-1), a key enzyme in the inflammatory response [12]. Both proteins and DNA in the human body possess chirality, establishing a unique chiral environment that imparts precise recognition of drug chirality. This phenomenon, termed stereoselectivity, results in distinct pharmacokinetics and pharmacodynamics for each enantiomer [11]. Consequently, in recent years, there has been a growing interest among researchers in investigating chiral resolution methods to obtain monochiral enantiomers [13–19]. Additionally, understanding the influence of conformational conversions is crucial in the investigation and clinical utilization of chiral drugs. Presently, research on the *in vivo* conversion of chiral drugs, such as FB, predominantly focuses on plasma [20,21], with limited exploration into other tissues, especially eye tissues. Thus, investigating the conversion of FB configuration within eye tissues holds immense significance for the clinical application and development of FB ophthalmic preparations, providing valuable insights to optimize therapeutic efficacy and safety for ocular conditions.

Beyond the impact of configuration on its activity, achieving efficient ocular drug delivery is crucial for the desired anti-inflammatory effect *in vivo*. The eye's surface presents several barriers that restrict drug delivery [22,23], including the corneal [24], conjunctival [25], and aqueous humor barriers [26,27]. The physical and chemical properties of drugs, such as molecular weight, size, charge, ionization, hydrophilicity, and lipophilicity, profoundly impact their ability to penetrate these barriers. FB, classified as a weak organic acid with a pKa of around 3.5–4.5, exhibits low water solubility and limited cornea permeability [28–30]. To enhance the local delivery efficiency of such drugs, specific penetration enhancement methods are required [31–33]. Moreover, the weak acidity of NSAIDs has the potential to irritate the cornea, resulting in conjunctival tingling and congestion [34]. These factors must be carefully considered to optimize the ocular delivery of FB and other NSAIDs, ensuring efficient drug delivery and minimizing possible ocular irritation.

In recent years, the quest for effective corneal penetration has given rise to various solutions, including the utilization of suitable drug carriers and penetration enhancers [9]. However, it is crucial to acknowledge that these strategies may impact the barrier function of the corneal epithelium, potentially leading to excipient-related toxicity and irritation [35,36]. Therefore, achieving a delicate balance between improving penetration efficiency and minimizing irritation becomes paramount to preserving the normal physiological function of the barrier. Ion pair technology has emerged as an effective strategy for modifying the physicochemical properties of drugs [37]. By combining two ions with opposite charges through coulomb attraction, ion pairing leads to the formation of ion pairs. This approach significantly increases the concentration of the unionized drug, enhancing its lipid solubility and facilitating permeability through the corneal epithelium [38]. Crucially, ion pairing does not alter the drug's mechanism of action, preserving its therapeutic effects. Another notable advantage of the ion-pair strategy is its potential to reduce eye irritation caused by drugs [39]. Through adjusting the physicochemical properties of the drug, ion pairing can mitigate irritation to a certain extent, thereby improving patient comfort during ocular administration. Moreover, ion pair technology brings several practical benefits to the forefront. Its implementation on a large scale ensures efficient and cost-effective production, making it an attractive option for drug development and manufacturing. Additionally, the technology is well-received by patients due to its improved drug efficacy and stability, enhancing its acceptability in clinical use.

To address the impact of chirality on the anti-inflammatory activity of FB, we employed chemical resolution to isolate and purify R-FB and S-FB. Additionally, to enhance the physicochemical properties, improve corneal permeability, and reduce irritation, FB was subjected to an ion-pair strategy with various counter-ions, such as sodium (Na), diethylamine (DEA), TMA, and l-arginine (ARG) [40–42]. Subsequently, a comprehensive comparison of the equilibrium solubility and oil-water partition coefficient of each enantiomer salt was conducted at different pH levels (5.8, 6.5, and 7.0). Furthermore, the *in vitro* corneal permeability of the enantiomer eye drop was thoroughly investigated. These findings suggest that S-FBTMA may be a promising candidate for further preclinical and clinical development in ocular drug delivery.

2. Materials and methods

2.1. Materials

Flurbiprofen (FB) was obtained from Aisi Pharmaceutical Co., Ltd. Enantiomerically pure (S)-(-)-α-methyl benzylamine (99% enantiomeric excess) was acquired from Shanghai Aladdin Biochemical Technology Co., Ltd., while (R)-(+)-α-methyl benzylamine (99% enantiomeric excess) was generously provided by Merck Ltd. The reference standards for both (R)-(-)-flurbiprofen (R-FB) and (S)-(+)-flurbiprofen (S-FB), with purity exceeding 99%, were graciously supplied by TRC (Toronto, ON, Canada). l-arginine, with a purity of 98%, was procured from Shanghai Macklin Biochemical Technology Co., Ltd. The prostaglandin E2 (PGE_2) test kit was acquired from Cloud-Clone Corp. Trometamol, with a purity of 99.5%, was obtained from Tianjin Damao Chemical Reagent Factory. Diethylamine, with a purity of 98%, was sourced from Tianjin Concord Technology Co., Ltd. A 0.01 M phosphate buffer solution (PBS) was procured from Yida Technology (Quanzhou) Co., Ltd. Arachidonic acid was obtained from Medbio Reagent Co., Ltd. Methanol, acetonitrile, and formic acid, all of LC–MS grade quality, were supplied by Fisher Scientific (Waltham, MA, USA). All remaining chemicals and solvents utilized were of analytical grade.

2.2. Separation of FB isomers

2.2.1. Separation of (R)-(-)-FB

In the synthesis process, 100.03 g (409.52 mmol) FB were dissolved in 900 ml methanol, followed by the gradual addition of 50.02 g (412.77 mmol) of (R)-(+)-α-methyl benzylamine. The resulting reaction mixture was stirred for 10 min, heated to 70 °C, and continued to stir for an additional 10 min. Subsequently, the solution was allowed to cool to room temperature and stirred overnight within a temperature range of 0–5 °C. The solution containing the crystals was then filtered and subsequently dried. The obtained crude product was dissolved by stirring with 9 times methanol (g/v), and the refined compound was obtained through two rounds of crystallization using the same method, yielding compound 3 [43] (Fig. 1).

To further modify compound 3, 10.31 g (28.21 mmol) of compound 3, 85 ml water, and 4.60 ml hydrochloric acid (HCl) (aqueous) were stirred for 30 min. The resulting mixture was filtered, washed with water until it reached a neutral pH, and subjected to two additional washes with 10 ml ethanol/water (1:5). After thorough drying, R-FB was obtained as a white solid.

2.2.2. Separation of (S)-(+)-FB

In the experimental procedure, 100.06 g (409.64 mmol) of FB were meticulously dissolved in 900 ml methanol. Subsequently, (S)-(-)-α-methyl benzylamine, totaling 50.14 g (413.76 mmol), was added dropwise. The resulting reaction mixture underwent 10 min of stirring, followed by heating to 70 °C, with continuous stirring for an additional 10 min. Afterward, the solution was gradually brought down to room temperature and stirred overnight within a temperature range of 0–5 °C. The solution containing the crystals was then filtered and subsequently dried. The crude product was dissolved by stirring with 9 times methanol (g/v), and the refined compound was obtained through two rounds of crystallization using the same method, resulting in the formation of compound 4 [43] (Fig. 1).

To further modify compound 4, 19.84 g (54.29 mmol) of compound 4, in combination with 150 ml water and 9 ml HCl (aqueous), were stirred for a duration of 30 min. The resulting mixture was subjected to filtration and washed with water until reaching a neutral pH. Two additional washes were performed using a 10 ml ethanol/water mixture (1:5). Following thorough drying, compound S-FB was obtained in the form of a white solid.

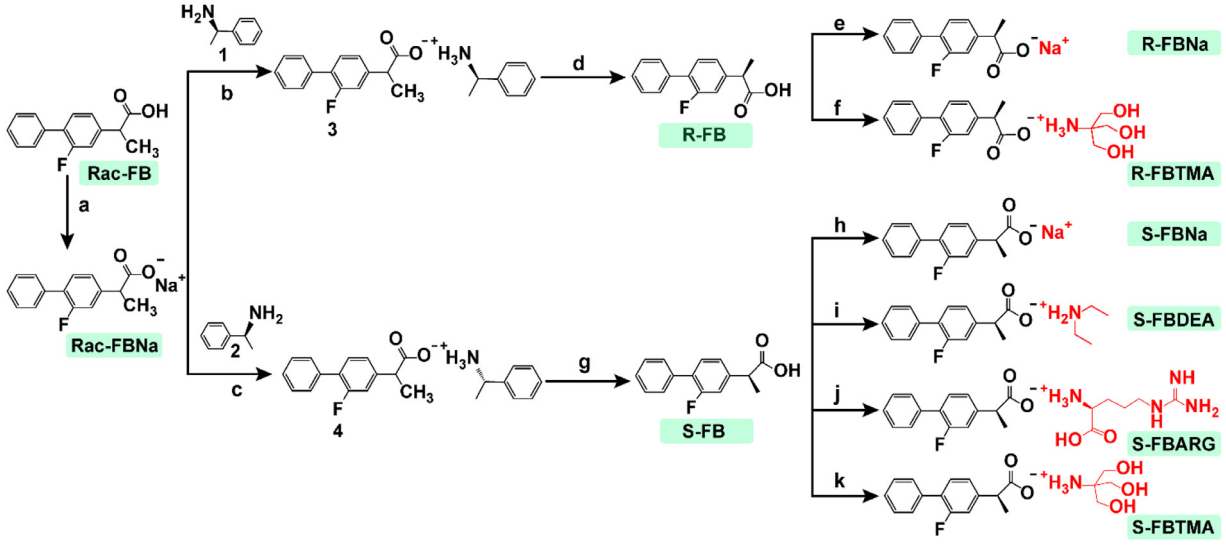

Fig. 1 – Synthetic routes for preparing the salts of FB: (a), (e), (h) NaOH; (d), (g) recrystallization, HCl (aq); (i), DEA; (j), ARG; (f), (k) TMA.

2.3. Synthesis of FB isomer corresponding salts

2.3.1. Synthesis of FBNa

In the experimental procedure, 10.05 g (41.14 mmol) of FB were meticulously dissolved in 90 ml acetone, followed by the gradual addition of a NaOH solution consisting of 1.64 g (41 mmol) dissolved in 20 ml water. The solvent was subsequently removed under vacuum using a rotary evaporator, and the resulting residue was washed with acetone/water (40:1) until reaching a neutral pH. The resulting solids were then dried to yield FBNa as a white solid.

2.3.2. Synthesis of S-flurbiprofen sodium (S-FBNa)

In the experimental procedure, 4.86 g (19.90 mmol) of S-FB were dissolved in 45 ml acetone, and subsequently, a NaOH solution consisting of 0.8 g (20 mmol) dissolved in 10 ml water was added dropwise. The resulting reaction mixture underwent crystallization, filtration, and subsequent washing with acetone/water (40:1) until it reached a neutral pH. The resulting solids were then dried, yielding S-FBNa in the form of a white solid.

2.3.3. Synthesis of R-flurbiprofen sodium (R-FBNa)

In the experimental procedure, 3.52 g (14.41 mmol) of R-FB was dissolved in 36 ml acetone, and subsequently, a NaOH solution containing 0.58 g (14.50 mmol) dissolved in 5 ml water was added dropwise. Following this addition, the reaction mixture underwent crystallization, followed by filtration and subsequent washing with an acetone/water mixture (40:1) until achieving a neutral pH. The resulting solid material was then dried, resulting in the formation of R-FBNa as a white solid.

2.3.4. Synthesis of S-flurbiprofen tromethamine (S-FBTMA)

In the experimental procedure, 5.02 g (20.55 mmol) of S-FB was meticulously dissolved in 45 ml acetone, and subsequently, a tromethamine solution containing 2.49 g (20.55 mmol) diluted in 10 ml water was added dropwise. The resulting reaction mixture was stirred at room temperature for 1 h, followed by concentration under vacuum using a rotary evaporator. The resulting crude product was washed with acetone/water (50:1) and then dried, yielding S-FBTMA as a white solid.

2.3.5. Synthesis of R-flurbiprofen tromethamine (R-FBTMA)

In the experimental procedure, 2.97 g (12.16 mmol) R-FB was dissolved in 27 ml acetone. Subsequently, a solution of trimethylamine (TMA) containing 1.48 g (12.22 mmol) diluted in 5 ml water was added dropwise. The resulting reaction mixture was stirred at room temperature for 1 h and then concentrated under vacuum. The crude product underwent washing with acetone/water (50:1) and subsequent drying, resulting in the formation of R-FBTMA as a white solid.

2.3.6. Synthesis of S-flurbiprofen diethylamine (S-FBDEA)

In the experimental procedure, 3 g (12.28 mmol) of S-FB were dissolved in 27 ml acetone. Subsequently, diethylamine (0.9 g, 12.3 mmol) was added slowly. The resulting reaction mixture was stirred at room temperature for 1 h, followed by the removal of acetone under vacuum using a rotary evaporator. This process yielded S-FBDEA as a yellow solid.

2.3.7. Synthesis of S-flurbiprofen arginine (S-FBARG)

In the experimental procedure, 5 g (20.47 mmol) of SFB was dissolved in 45 ml acetone. Subsequently, a solution of arginine (ARG) comprising 3.57 g (20.49 mmol) dissolved in 30 ml water was added dropwise. After stirring at room temperature for 1 h, the reaction was terminated. The solvent was then removed under vacuum using a rotary evaporator, resulting in the formation of S-FBARG as a milky white semisolid.

2.4. Characterization of FB and its salts

2.4.1. Circular dichroism (CD)

For optical configuration characterization, suitable quantities of R-FB and S-FB were dissolved in PBS. Subsequently, a circular dichroism spectrometer (J-815, JASCO Corporation) was employed for measurements within the wavelength range of 200–400 nm [44]. The CD spectral data were processed using Spectra Manager software.

2.4.2. Mass spectrometry (MS)

We accurately weighed and dissolved appropriate quantities of R-FB and S-FB in methanol. The analysis was conducted using a SolariX 7.0T Instrument (Bruker Daltonic Inc.) operating in electrospray ionization (ESI)-negative mode with a source temperature of 200 °C. The scan range encompassed 100–1,200 *m/z*.

2.4.3. Nuclear magnetic resonance spectroscopy (NMR)

The ^{1}H NMR (400/600 MHz) and ^{13}C NMR (100/150 MHz) spectra of FBNa, S/R-FBNa, S/R-FBTMA, S-FBDEA, and S-FBARG were acquired in deuterated dimethyl sulfoxide (DMSO–d6) or deuterated methanol (MeOD) using a Bruker nuclear magnetic resonance spectrometer (Bruker BioSpin GmbH). The measurements were conducted at a temperature of 298 K. Chemical shift values (δ) were expressed as ppm, and coupling constants (*J*) in hertz. Data interpretation was carried out using the MestReNova software.

2.4.4. Fourier transform infrared spectroscopy (FTIR)

Weighed quantities of S-FB, S-FBNa, and S-FBTMA were individually combined with KBr and subsequently pressed into tablets. The infrared spectra of each mixed tablet were then recorded using an FTIR spectrometer (Thermo Scientific Nicolet iS20) at room temperature within the range of 4000–400 cm^{-1}, employing a resolution of 2 cm^{-1} [45].

2.4.5. Scanning electron microscopy

FB and its isomer salts underwent examination via scanning electron microscopy (SEM) using a Regulus 8100 instrument from Hitachi, Japan. Prior to analysis, the samples were coated with gold, and the SEM was operated with an accelerated voltage of 3 kV.

2.4.6. Viscosity

The Pinner capillary viscometer was vertically secured in a water bath with a constant temperature set at 20 °C. Eye drops from the FB groups were dispensed to allow natural falling within the tube. The flow time of the liquid level from the measurement line m_1 to the measurement line m_2 was

meticulously recorded using a stopwatch. The measurement process was repeated three times following the specified protocol, and the overall average value was calculated using the following formula, representing the dynamic viscosity of the eye drops [46]:

$$\eta = Kt \times \rho$$

Here, η represents dynamic viscosity, K is the known viscosity meter constant for standard liquid viscosity measurement (units: mm^2/S^2), t denotes the measured average flow time in s, and ρ is the density of the tested substance at the same temperature in g/cm^3.

2.5. *Preparation of ophthalmic solutions*

Referring to the prescribing information for FBNa eye drops (Ocufen®, 0.03%), the FB and each isomer eye drops were prepared in the laboratory as follows: To obtain a 4% polyvinyl alcohol solution, 4 g polyvinyl alcohol was weighed and placed in a beaker, and 100 ml water was added. The mixture was agitated at 85 °C for 1 h and then placed at room temperature for 12 h to remove bubbles. Active pharmaceutical ingredients (APIs), citric acid, sodium citrate, sodium chloride, and potassium chloride were weighed and deposited in a beaker according to the prescription. Sterile water (50 ml) was added and dissolved using ultrasonic energy. The pH was then adjusted to 6.0–7.0 with 0.1 mol/l HCl following the addition of 35 ml of 4% polyvinyl alcohol solution. Finally, sterile water was added to make up the volume to 100 ml. To obtain ocular drops, the above liquid was filtered through a 0.45 μm microporous membrane and then a 0.22 μm microporous membrane [47]. The osmotic pressure was measured at 280–360 mOsmol/kg using a STY-1ADK osmometer (Tianjin Tiandatianfa Technology Co., Ltd.) following the freezing point drop principle.

2.6. *Animal study*

Healthy male Japanese white rabbits (SYXK (Liao) 2018–0009) weighing 2 to 2.5 kg were obtained from Liaoning Changsheng Biotechnology Co., Ltd (Benxi, China) and housed in a controlled animal facility maintained at a temperature of 20 °C to 25 °C and relative humidity ranging from 40% to 75%. These rabbits were provided with unrestricted access to a balanced diet of pellets and water. Prior to the commencement of the trial, all animals underwent rigorous screening to confirm the absence of any eye diseases or irritation symptoms. The animal study protocol was subjected to approval by the Institutional Animal Ethical Care Committee (IAECC) of Shenyang Gerunsite (CSE202206012; dated 18 June 2022).

2.7. In vivo *chiral pharmacokinetics*

Sixty male Japanese white rabbits were randomly divided into three groups, each consisting of 20 rabbits. These groups were administered different formulations: Ocufen® eye drops, S-FBNa 0.03% eye drops, and R-FBNa 0.03% eye drops. Instillation involved administering 100 μl the respective eye drops into both eyes of each rabbit, followed by manual closure of the eyelids for one min to prevent potential overflow of the instilled drug solution. Euthanasia was performed at specified time intervals of 0.25, 0.5, 0.75, 1, 1.5, 2, 4, 6, 8 and 10 h post-administration. Tear samples were collected using paper strips and weighed at each time point. Additionally, approximately 150 μl aqueous humor was extracted from the anterior chamber of each rabbit's eye using a 1 ml syringe. Subsequently, the eyelid conjunctiva and the eyeball were excised, with the iris and cornea dissected from the eyeball [48]. These separate samples were collected, weighed, and immediately stored at −80 °C until subsequent analysis via high-performance liquid chromatography–tandem mass spectrometry (HPLC–MS/MS) (Shimadzu, Kyoto, Japan).

2.8. *Equilibrium solubility studies*

In 5 ml PBS, surplus quantities of FBNa, S-FBNa, S-FBDEA, S-FBARG, S-FBTMA, and R-FBNa were introduced into stoppered glass test tubes at varying pH levels (5.8, 6.5 and 7.0). Ultrasonication was employed for 30 min to ensure complete dissolution until the solutions reached a state of supersaturation. Each sample was replicated three times in parallel at each pH condition. Following 72 h of incubation at 37 °C, the samples were extracted and subjected to centrifugation at 12,000 rpm for 10 min [49]. The resulting supernatant was filtered through a 0.22 μm microporous membrane, and the filtrate was subsequently diluted with acetonitrile/water/glacial acetic acid (60:40:0.1, v/v/v) before injection into the HPLC system for analysis.

2.9. *Determination of $lgP_{o/w}$*

In a sealed triangular flask, n-octanol was combined with isovolumetric PBS solutions at pH levels of 5.8, 6.5 and 7.0. After 24 h of incubation at 37 °C, the two phases achieved thorough saturation. Following static stratification, these phases were separated and stored individually. FBNa, S-FBNa, S-FBDEA, S-FBARG, S-FBTMA, and R-FBNa were each fully dissolved in 3 ml water-saturated n-octanol solution, followed by the addition of 3 ml n-octanol-saturated aqueous solution. The solution was then incubated until equilibrium was reached at 37 °C. Three samples were simultaneously collected from each group. After 72 h, the samples underwent centrifugation at 12,000 rpm for 10 min, and the resulting supernatant was filtered through a microporous membrane with a pore size of 0.22 μm [50]. The filtrate was subsequently diluted using an acetonitrile/water/glacial acetic acid mixture (60:40:0.1, v/v/v). The distribution coefficient (*D*) was calculated using the following equation.

$$\log P_{ow} = \log\left(\frac{C_o}{C_w}\right) \quad (1)$$

where C_o represents the drug concentration in n-octanol-saturated water, and C_w signifies the drug concentration in water saturated with n-octanol.

2.10. In vitro *corneal permeation studies*

The evaluation of corneal penetration was conducted using isolated rabbit corneas, which were excised from sacrificed

rabbits and immersed in preheated glutathione bicarbonate - Ringer's solution (GBR) at 35 °C before being employed in Franz vertical cells for testing. The receptor chamber was filled with 7.8 ml GBR solution, with an effective penetration area of 0.78 cm^2. The isolated corneas were securely positioned between the donor and receptor chambers, with the epithelium facing the donor. Subsequently, 1 ml of 0.015% R-FBNa eye drops, 0.015% S-FBNa eye drops, and 0.018% S-FBTMA eye drops were introduced into the respective donor chambers. The cells were maintained at a temperature of 35 °C with continuous thermostatic magnetic stirring. Samples were collected from the receptor chamber at 40, 80, 120, 160, 200 and 240-min intervals, each time extracting 0.5 ml, followed by replenishing the same volume of preheated fresh GBR solution [48,51]. All experiments were performed in triplicate and analyzed using HPLC.

In this study, the cumulative penetration quantity (Q_n, μg/cm^2) was calculated as follows:

$$Q_n = \frac{V_0}{A}(C_n + \frac{V}{V_0}\sum_{i=1}^{n-1} C_i) \quad (2)$$

Where C_n represents the measured drug concentration in the endothelial compartment at different intervals (μg/ml), C_i is the measured drug concentration before time t (μg/ml), V_0 is the volume of the solution in the receptor chamber (ml), V is the sampling volume (ml), and A is the effective penetration area (cm^2).

The apparent permeability coefficient (P_{app}, cm/s) was calculated as follows:

$$P_{app} = \frac{\Delta Q}{\Delta t C_0} \quad (3)$$

Where C_0 is the initial drug concentration in the donor cell, and $\Delta Q/\Delta t$ is obtained from the slope rate of the linear portion on the Q_n – t plot.

The steady-state flux (J_{ss}, μg/(cm^2·s)) was calculated as follows:

$$J_{ss} = C_0 \bullet P_{app} \quad (4)$$

2.11. In vivo *pharmacokinetic of S-FBTMA*

In this study, a cohort of 20 male Japanese white rabbits was subjected to testing. The experimental group received S-FBTMA 0.036% eye drops. Each rabbit received 100 μl the corresponding eye drops instilled into both conjunctival sacs, followed by manual closure of the eyelids for 1 min to prevent any potential overflow of the administered drug solution. At specified time intervals of 0.25, 0.5, 0.75, 1, 1.5, 2, 4, 6, 8 and 10 h post-administration, tear samples were collected using paper strips and their weights were recorded. Additionally, approximately 150 μl aqueous humor was extracted from the anterior chamber of each rabbit's eye using a 1 ml syringe. The removal of eyelid conjunctiva and eyeball was followed by the dissection of the iris and cornea from the eyeball [47,48]. Separate samples were carefully collected, weighed, and immediately preserved at −80 °C until further analysis by LC–MS [52].

2.12. *Ocular anti-inflammation efficiency*

Inflammation represents an exaggerated immune response of body tissues to both physiological and pathological stimuli. This response is intensified through the activation of inflammatory cells and the production of inflammatory factors. Specifically, cell membrane phospholipids generate arachidonic acid (AA) upon the activation of phospholipase A2. Free AA, in turn, can be catalyzed by COX to produce various prostaglandins (PG) and prostacyclin (PGI). Prostaglandins have the potential to compromise the ocular blood–aqueous barrier, elevate vascular permeability, induce leukocytosis, and elevate intraocular pressure [53]. This process leads to noninfectious inflammatory reactions in the eye, resulting in prolonged inflammation. Therefore, researchers commonly employ arachidonic acid (AA) to induce inflammatory models [6,54].

To assess the ocular anti-inflammatory effects of FB formulations utilizing an arachidonic acid-induced inflammation model, a total of 30 rabbits were randomly allocated into different groups: Ocufen® eye drops group, S-FBTMA 0.036% eye drops group, R-FBTMA 0.036% eye drops group, PBS group, and a normal group.

At the commencement of the experiment, rabbits in both the PBS group and the drug administration group received 100 μl PBS or the corresponding drugs in the conjunctival sac of their left eye, respectively, while the right eye remained untreated. After a 0.5-h interval, 50 μl of a 0.5% (w/v) arachidonic acid solution was instilled into the conjunctival sac of the left eye of each rabbit to induce the inflammatory model. Subsequently, at 0.5 h post-modeling, 100 μl PBS or the corresponding drugs were administered to the left conjunctival sac of the rabbits in each group. At 7.5 h post-modeling, the left eyes of all rabbits were assessed using the Draize test to determine the severity of eye inflammation. Following scoring, the rabbits' eyes were rinsed three times with 150 μl PBS from the upper eyelid, and samples were collected from the lower eyelid using a 0.9 mm capillary tube and stored at −20 °C. The degree of inflammation in the rabbit's eyes was further evaluated through an enzyme-linked immunosorbent assay (ELISA) for the quantitative measurement of prostaglandin E2 levels (pg/ml) in tears [55,56].

Following tear extraction, the animals were euthanized to assess the impact of eye drops on the recovery of rabbit eye tissue post-drug administration. The eyeballs were extracted, rinsed with 0.9% (w/v) sodium chloride, and then fixed in a 10% (w/v) formalin solution. Hematoxylin and eosin (H&E) staining were employed for pathological investigation under a microscope.

2.13. *Ocular irritation test*

To evaluate the ocular safety of FB, a total of 15 rabbits were randomly divided into five groups: the Ocufen® eye drops group, S-FBTMA 0.036% eye drops group, R-FBTMA 0.036% eye drops group, a negative control group (comprising blank eye drops without active ingredients), and a blank group. Over the course of seven consecutive d, each group of rabbits received instillations of 100 μl in their left eyes four times a d. At one-h

intervals after the last administration of each dose, the cornea, iris, and conjunctiva were examined macroscopically using a slit light.

The ocular Irritation level was assessed using the Draize test [57,58], with the following scoring criteria: no irritation (0–3 points); mild irritation (4–8 points); moderate irritation (9–12 points); and severe irritation (or corrosive, scoring 13–16 points).

2.14. *Statistical analysis*

Statistical analysis was conducted using the student's *t*-test for comparisons involving two groups and the ANOVA test for those involving multiple groups. The analysis was carried out using GraphPad InStat Demo Version (GraphPad Software, Inc., San Diego, USA). All quantitative data are expressed as the mean ± standard deviation (SD). Statistical significance was established at a threshold of $P < 0.05$.

3. Results and discussion

3.1. *Synthesis and characterization of R/S-FBNa*

Firstly, the chiral resolution of FB was performed by chemical resolution method. The routes of chiral resolution are shown in Fig. 1. The successful separation of R-FB and S-FB was confirmed by MS (Figs. S1–S2) and CD spectra (Fig. S3). The CD spectra showed four strong signal peaks at 206 nm, 218 nm, 243 nm, and 275 nm in the test range of 200–400 nm, indicating that the isomers have obvious optical activity. Among them, R-FB showed a positive Cotton effect (CE) at 206 nm, 243 nm, and 275 nm, and a negative signal at 218 nm, while the signal of S-FB was completely opposite, indicating that the two were enantiomers. The purity of R-FB and S-FB was determined by peak area normalization using HPLC. The purity of R-FB and S-FB was 99.44% and 99.60%, respectively. Then, the sodium salt of rac-FB and R/S-FB (rac-FBNa, R-FBNa and S-FBNa) was synthesis (Fig. 1). The chemical structures of rac-FBNa, R-FBNa and S-FBNa were confirmed by ^{1}H NMR and ^{13}C NMR (Figs. S4–S6). The purity of rac-FBNa, R-FBNa and S-FBNa was 99.83%, 99.71% and 99.84%, respectively.

3.2. In vivo *stereoselectivity and configurational conversion*

Numerous studies have consistently demonstrated enhanced activity associated with the S configuration. Therefore, a critical investigation into *in vivo* stereoselectivity and configurational conversion is imperative. In this section, we conducted an assessment of FB levels in various ocular tissues, including aqueous humor (AH), iris, conjunctiva, cornea, and tears, utilizing Japanese big-ear white rabbits to elucidate stereoselective behavior and conformational conversion *in vivo*. As depicted in Figs. 2A–2C and S7–S8, and Tables S1–S5, our analysis reveals a noticeable absence of statistically significant distinctions in key pharmacokinetic parameters, comprising area under the curve (AUC(0-t)), maximum concentration (C_{max}), peak concentration time (T_{max}), and half-life period ($T_{1/2}z$), across rac-FBNa, S-FBNa, and R-FBNa at the 0.03% concentration level when administered individually. This observation suggests that, under equivalent concentration conditions, the pharmacokinetic profiles of R-FBNa 0.03%, S-FBNa 0.03% eye drops, and the rac-FBNa 0.03% group do not exhibit stereoselectivity.

In addition, the conversion of R-FB to S-FB in aqueous humor, iris, conjunctiva, cornea, and tear was measured within 0.25 to 10.0 h after administration of 0.03% R-FBNa. As shown in Figs. 2D–2F, and S7–S8 and Tables S6–S10, the conversion rate from R-FB to S-FB in aqueous humor, iris, conjunctiva, cornea, and tear was 14.77%, 8.90%, 11.86%, 16.69%, and 3.0%, respectively. The aforementioned findings substantiate the lack of discernible stereoselectivity and conformational conversion *in vivo* between the R-FB and S-FB configurations. This validation underscores the meaningfulness of pursuing chiral separation strategies. In summary, there is no stereoselectivity between the R and S configurations and a minimal conformational conversion. We hypothesize that both rac-FBNa and S-FBNa primarily enter the eye through passive diffusion. At a consistent concentration of 0.03%, the pharmacokinetic parameters of rac-FBNa and S-FBNa exhibit similarity, with no discernible statistical difference, indicating an absence of pharmacokinetic selectivity between the two. The substitution of S-FBNa for rac-FBNa establishes a foundation for understanding pharmacokinetics in this context.

3.3. *Synthesis and characterization of S-FB corresponding salts*

As a weakly acidic drug, FB has low water solubility, poor corneal permeability and high irritation, which seriously hinders its delivery efficiency *in vivo* and easily causes large side effects. In order to further improve its undesirable physical and chemical properties, we adopted the ion pair strategy to modify its structure. Considering the high pharmacological activity of S-FB, we further synthesized a variety of S-FB corresponding salts using DEA, TMA and ARG as a counter ion. The synthesis routes are shown in Fig. 1. The successful synthesis of S-FBDEA, S-FBTMA and S-FBARG was confirmed by ^{1}H NMR and ^{13}C NMR (Figs. S9–S11). The purity of S-FBDEA, S-FBTMA and S-FBARG was 99.34%, 99.50% and 99.33%, respectively. The notable chemical shifts for rac-FBNa, S-FBNa, and S-FBTMA were observed at H-13 and H-14 (Table S17), with identical coupling constants. Additionally, the chemical shift at 3.42 for S-FBTMA corresponds to the CH_2 group of trometamol.

Following this, an analysis of the IR spectrogram was conducted. As depicted in Fig. S15, the O–H stretching vibrations and out-of-plane bending vibrations are indicated by bands between 2500 and 3400 cm^{-1}, with a unique characteristic peak at 925 cm^{-1} in the FTIR spectra of S-FB. The stretching vibration of C=O is observed at 1731 cm^{-1}, while the dimer's stretching vibration of C=O is identified at 1696 cm^{-1}. Distinctive peaks at 1621 cm^{-1} and 1511 cm^{-1} are attributed to the skeletal vibrations of the aromatic ring. Additionally, 2977 cm^{-1}, 1461 cm^{-1}, and 1390 cm^{-1} represent stretching vibrations, asymmetric bending vibrations, and symmetric bending vibrations of $-CH_3$, respectively [45]. The

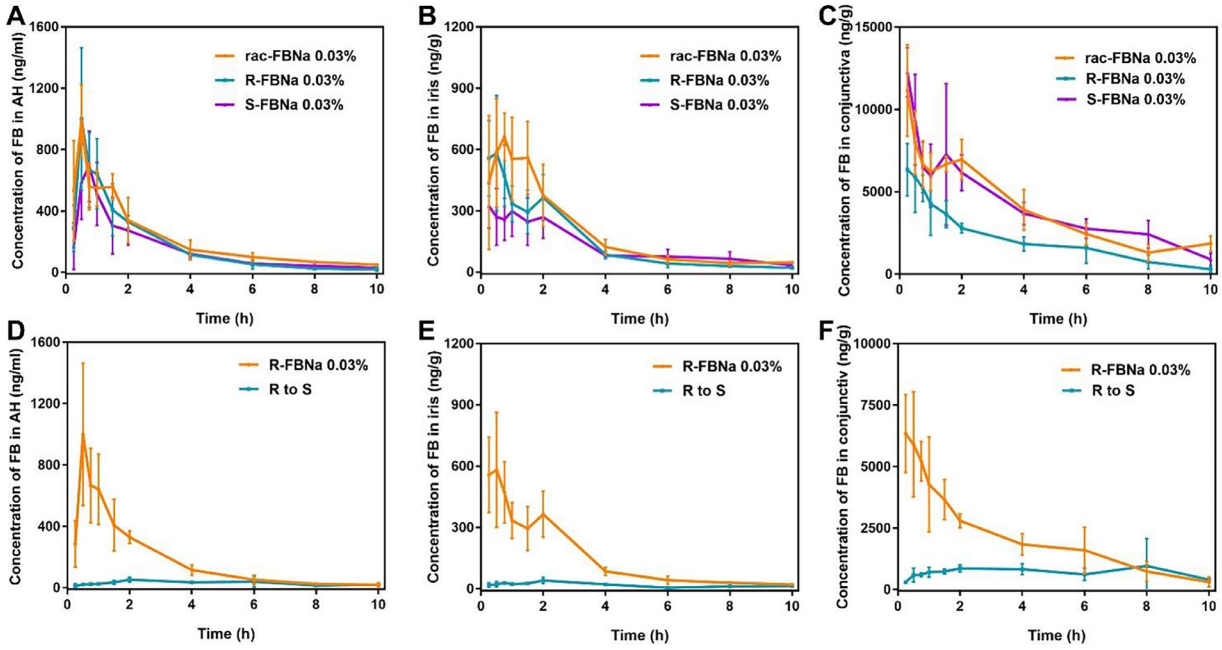

Fig. 2 – *In vivo* stereoselectivity and configurational conversion. The concentration-time curves following a single dose administration of rac-FBNa 0.03%, R-FBNa 0.03% and S-FBNa 0.03% in AH (A), iris (B) and conjunctiva (C). R-FBNa convert to S isomer in AH (D), iris (E) and conjunctiva (F). The data are presented as the mean ± SD ($n = 4$).

disappearance of the absorption peak at 1731 cm^{-1} for C=O, along with the emergence of new peaks at 1555 cm^{-1} and 1407 cm^{-1} for S-FBNa, and 1559 cm^{-1} and 1401 cm^{-1} for S-FBTMA, 1555 cm^{-1} and 1417 cm^{-1} for S-FBDEA, and 1551 cm^{-1} and 1392 cm^{-1} for S-FBARG, is attributed to the asymmetric and symmetric modes of COO^{-}. These alterations in the FTIR spectra serve as compelling evidence confirming the formation of FB salts [59,60].

Morphological analysis of the shape and surface of FB isomer salts was initially conducted through SEM assessment. Fig. S14 displayed distinctly different surface morphologies among the FB isomer salts, indicating variations in their crystalline phases [45]. The viscosity of FB ophthalmic formulations was measured, and the results are presented in Table S20. It is evident from the data that the viscosity of our formulations falls within the appropriate range of 4.0–5.0 mm^2/S^2.

3.4. *Physicochemical properties of FB salts*

Ocular pharmaceutical agents can exert their therapeutic effects solely upon traversing the corneal barrier and reaching the anterior segment of the eye. The corneal permeability of drugs is contingent upon their inherent physicochemical attributes, including water solubility and lipid solubility. Consequently, we embarked on the assessment of the equilibrium solubility and oil–water partition coefficient ($lgP_{o/w}$) of FB salts, as these parameters play pivotal roles in this context. The results of the equilibrium solubility assessments are depicted in Fig. 3A–3C. The findings from these equilibrium solubility tests, conducted at pH levels of 5.8, 6.5, and 7.0, reveal a consistent pattern of increasing solubility for each isomeric salt with ascending pH values, aligning with the dissolution behavior typically observed in weakly acidic nonsteroidal anti-inflammatory drugs (NSAIDs). Within the pH range of 5.8–7.0, S-FBARG exhibited the highest solubility among the FB salts. Notably, the solubility of S-FBTMA displayed a more pronounced pH-dependent increase compared to that of S-FBNa. At pH 6.5, the solubility ranking of the isomeric salts was as follows: S-FBNa < FBNa < S-FBTMA < R-FBNa < S-FBDEA < S-FBARG.

Moreover, we assessed the oil-water partition coefficient ($lgP_{o/w}$) of the various FB salts across distinct pH values, and the outcomes are delineated in Fig. 3D–3F. Of particular note, the $lgP_{o/w}$ of S-FBARG exhibited values below 0, which signified low lipid solubility. This characteristic was unfavorable for effective corneal penetration. Contrastingly, S-FBTMA demonstrated maximal $lgP_{o/w}$ values at all three pH levels, signifying superior lipid solubility. At pH 6.5, the $lgP_{o/w}$ ranking for the isomers was as follows: S-FBARG < R-FBNa < S-FBNa < S-FBDEA < FBNa < S-FBTMA. Specifically, S-FBTMA maintained $lgP_{o/w}$ values ranging from 1.44 to 3.02 within the pH range of 5.8 to 7.0, rendering it more amenable to penetration through amphiphilic corneal tissues. Taking into account both equilibrium solubility and oil-water partition coefficient assessments for the FB salts, it is noteworthy that, at pH 6.5, the solubility of S-FBTMA (4,396.11 μg/ml) surpassed that of FBNa (3,096.70 μg/ml) and S-FBNa (2,563.22 ± 28.95 μg/ml) by 41.96% and 71.51%, respectively. Furthermore, the lipid solubility of S-FBTMA exhibited a notable increment of 12.68% and 24.03%.

3.5. In vitro *corneal permeation*

The enhanced solubility and lipid affinity observed may potentially augment corneal permeability and, consequently

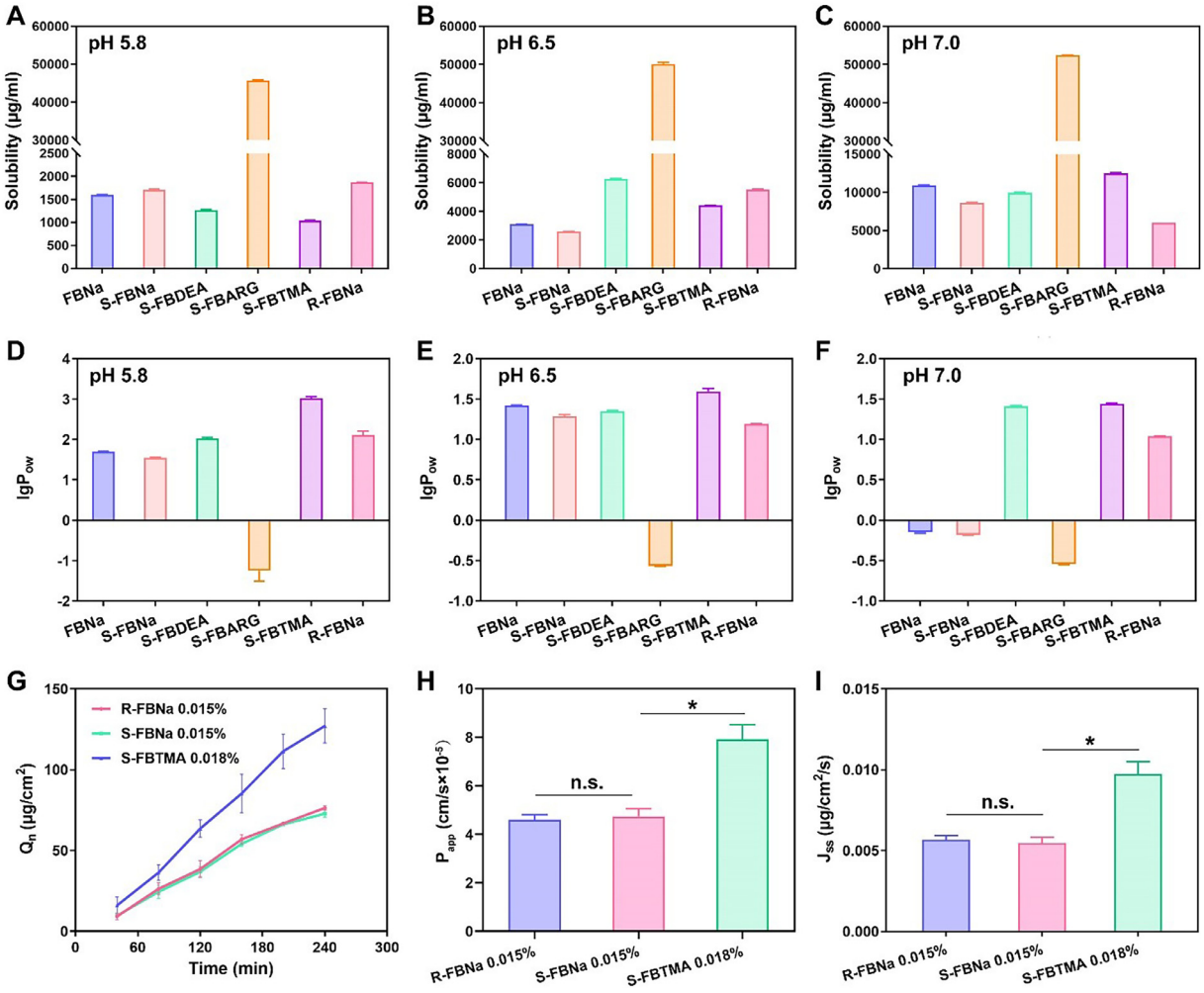

Fig. 3 – Physicochemical property of FB salts and *in vitro* corneal permeation study. The equilibrium solubility of FB salts in pH 5.8 (A), pH 6.5 (B), and pH 7.0 (C) at 37 °C. The lg P_{ow} of FB salts in pH 5.8 (D), pH 6.5 (E), and pH 7.0 (F) at 37 °C. *In vitro* corneal permeation profiles, Q_n (G), P_{app} (H) and J_{ss} (I) of different FB isomer. The data are presented as the mean ± SD ($n = 3$). *$P < 0.05$.

enhance ocular bioavailability. Therefore, we investigated *in vitro* corneal permeability of various FB salts by measuring the cumulative penetration quantity per area (Q_n), apparent permeability coefficient (P_{app}) and steady-state flux (J_{ss}). The corneal penetration profiles for three FB isomer eye drops (R-FBNa 0.015%, S-FBNa 0.015%, S-FBTMA 0.018%) are depicted in Fig. 3G–3I. As shown in Fig. 3G, three FB isomer eye drops exhibited a nearly constant rate of corneal penetration, with cumulative penetration amounts demonstrating a robust linear correlation with time ($R^2 > 0.98$). Upon reaching the 240 min mark, the cumulative permeation quantities for S-FBNa 0.015% eye drops and R-FBNa 0.015% eye drops were 72.79 and 73.38 μg/cm^2, respectively, indicating no significant disparity between the two groups. Likewise, there were no discernible differences in P_{app} or J_{ss} between these two groups (Fig. 3H–3I). In contrast, the Q_n for S-FBTMA 0.018% eye drops measured 127.09 ± 10.54 μg/cm^2, representing a substantial 76% increase compared to S-FBNa 0.015% eye drops (72.79 ± 2.40 μg/cm^2), with statistical significance ($P < 0.05$). Furthermore, both P_{app} and J_{ss} exhibited increments of 67% and 78%, respectively, with statistical significance. In summary, the above results suggested that TMA, as compared to sodium salt, exerted a more pronounced enhancing effect on the corneal permeability of S-FB. This phenomenon could be attributed to the formation of ion pairs between TMA and S-FB, thereby enhancing its lipophilicity and hydrophilicity, facilitating its passage through the amphiphilic corneal tissue.

3.6. In vivo *pharmacokinetic and tissue distribution*

In light of the favorable *in vitro* corneal permeability of S-FBTMA, we proceeded to investigate its pharmacokinetic behavior and ocular distribution *in vivo*. As depicted in Fig. 4A and 4B, C_{max} and AUC of S-FBTMA 0.036% exceeded those of S-FBNa 0.03%, both in the aqueous humor and iris. This discrepancy suggested that the ion pair formed between TMA and S-FB augmented its solubility in both aqueous and lipid environments, facilitating its passage through the amphiphilic corneal barrier and into the aqueous humor. Consequently, the drug concentration in the aqueous humor

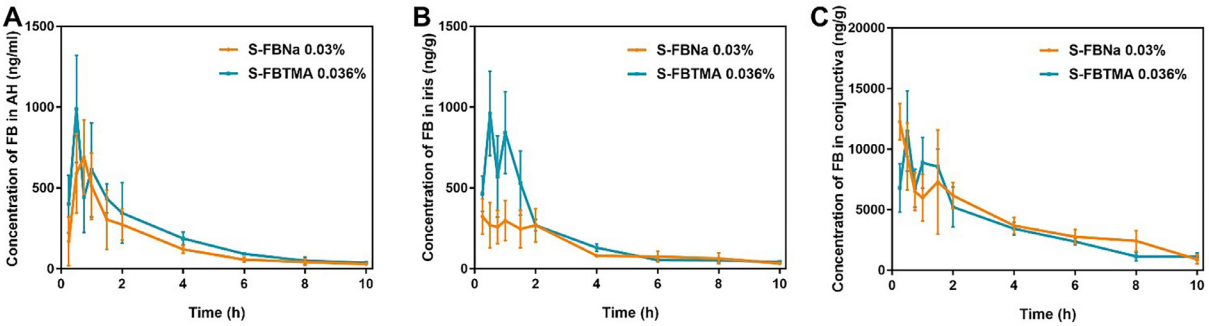

Fig. 4 – Ocular pharmacokinetic profile of S-FBTMA in AH (A), iris (B) and conjunctiva(C) after single-dose administration. The data are presented as the mean ± SD ($n = 4$).

was elevated, subsequently influencing its distribution within the iris. The phenomenon was consistent with the outcomes of the *in vitro* corneal penetration assessments. In addition, there was no significant difference between the C_{max} and AUC of S-FBTMA 0.036% and S-FBNa 0.03% in conjunctiva, tears and cornea (Figs. 4C and S12). It is conceivable that the conjunctiva, situated on the ocular surface, primarily serves as a rapid exit route for a significant portion of the administered drugs, as they are swiftly drained through the nasolacrimal duct subsequent to eye drop instillation. Furthermore, the continual washing effect of tears, coupled with the limited contact duration between the drug and the conjunctival tissue, may lead to inadequate drug absorption in this region. The results indicate that, in comparison to S-FBNa 0.03%, the levels of S-FBTMA 0.036% detected in the aqueous humor and iris were elevated by 43.69% and 64.61%, respectively. This suggests that S-FBTMA 0.036% may exhibit enhanced therapeutic potential and possess advantageous attributes as a newly developed medication.

3.7. *Ocular anti-inflammation efficiency*

Ocular inflammation and inflammatory symptoms were quantified 7 h after the last instillation of FB formulations (Fig. 5A). The negative control exhibited no anti-inflammatory effect, resulting in severe conjunctival redness and swelling, accompanied by a substantial quantity of secretion, and receiving high clinical scores (Fig. 5B and 5C). The commercial FBNa 0.03% group showed a limited reduction in ocular inflammatory symptoms, remission of conjunctival redness and edema, and a small amount of secretion. When the eyes were treated with R-FBTMA 0.036%, the remission of conjunctival redness and swelling was greater than in the FBNa 0.03% group, and produced more secretion. S-FBTMA 0.036% significantly reduced conjunctival congestion, edema, and ocular surface secretion, outperforming FBNa 0.03% and R-FBTMA 0.036%, and scored lower than R-FBTMA and FBNa 0.03% (Fig. 5B and 5C).

In addition, the anti-inflammatory effect was further evaluated by measuring the levels of inflammatory factors (Fig. 5D). The level of PGE_2 in the negative control group increased significantly when compared to the normal group, indicating that the model was successful. The concentration of PGE_2 slightly decreased in tears after treatment with R-FBTMA 0.036%, which verified that R-FBTMA 0.036% had a limited effect on blocking the synthesis of PGE_2 during the development of ocular inflammation. In addition, the concentration of PGE_2 after treatment with S-FBTMA 0.036% was the lowest, significantly better than that of the R-FBTMA 0.036% group and the positive control group (FBNa 0.03%), indicating that S-FBTMA had higher anti-inflammatory activity than FBNa. Based on the above results, S-FBTMA 0.036% demonstrated effectiveness in preventing and treating conjunctivitis, providing a basis for clinical development.

To further assess the impact of various eye drop formulations on ocular tissues, conjunctiva samples from rabbit eyes were collected at the treatment endpoint, and conjunctival cell structure and tissue integrity were examined using H&E staining (Fig. 5E). In the normal group, epithelial cells were well-oriented, displaying no noticeable cytolysis or structural loss. Moreover, the glandular and fibrous layers showed no significant infiltration of inflammatory cells, including mast cells. In the model group, epithelial layer cells were irregularly arranged, exhibiting cell degeneration, lysis, and structural loss. The glandular layer displayed substantial infiltration of inflammatory cells, leading to a blurred border with the epithelial layer, and mast cells were evident in the fibrous layer. These findings indicated a substantial inflammatory response in the conjunctival tissue. In the FBNa 0.03% group (Fig. 5E), the boundary with the epithelial layer was clear, and no mast cells were observed in the fibrous layer. The R-FBTMA 0.036% group exhibited erratic organization of epithelial layer cells, with no considerable reduction in cell lysis, degeneration, and structural loss compared to the model group. The border with the epithelial layer was blurred, and a notable number of inflammatory cells were still present in the glandular and fibrous layers. In the S-FBTMA 0.036% group, epithelial cells were regularly arranged, showing significantly less cell degeneration, lysis, and structural loss than the model group. Moreover, the glandular and fibrous layers did not exhibit significant infiltration of mast cells or other inflammatory cells. The organization of epithelial layer cells was cleaner and denser compared to the FBNa 0.03% group (Fig. 5E).

3.8. *Ocular irritation of FB*

The results of the eye irritation assessment, conducted using the modified Draize test (Fig. 5F), indicated that no discernible irritation was observed in the negative control group. In

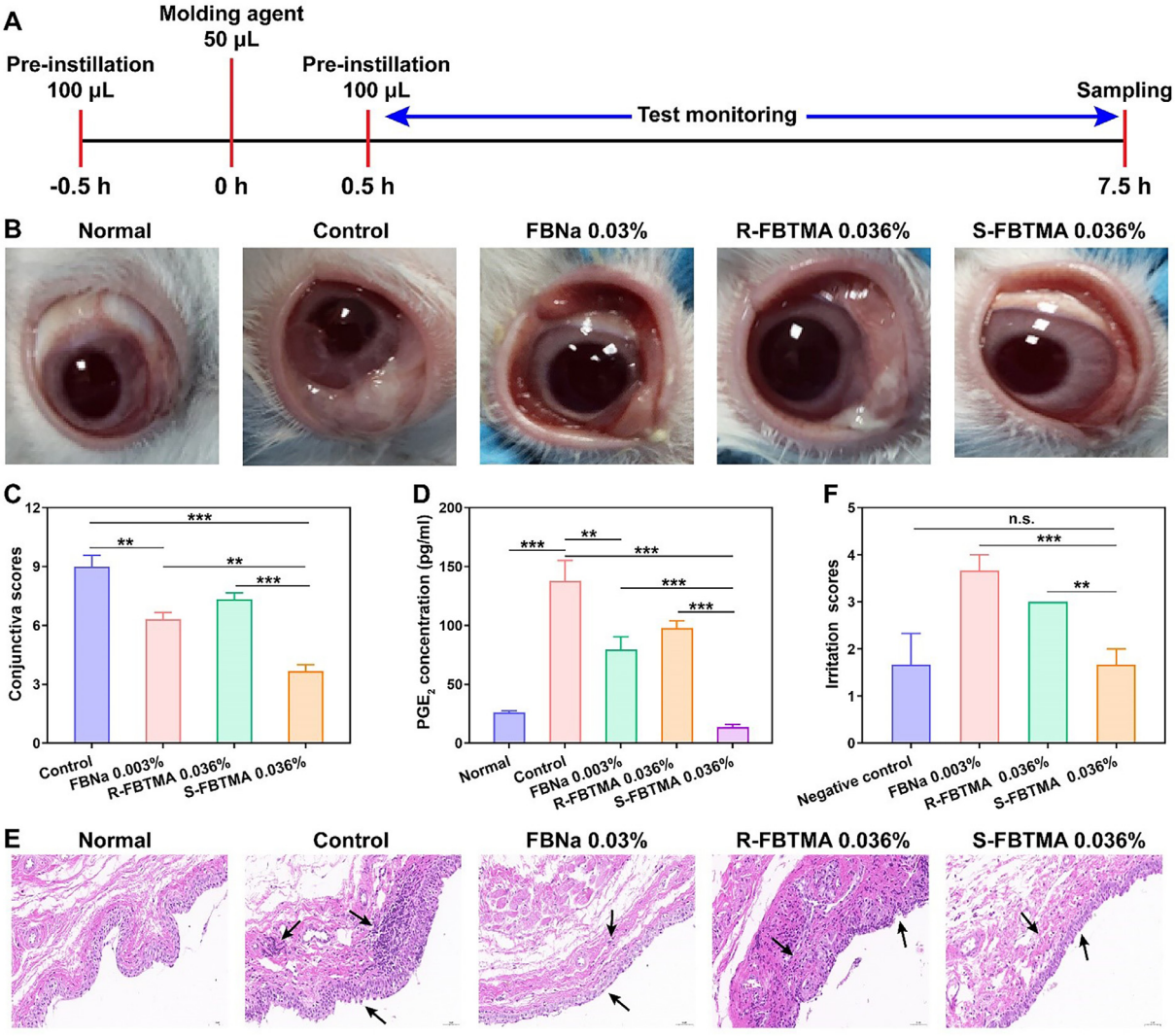

Fig. 5 – *In vivo* anti-inflammation efficiency and ocular irritation. (A) Timeline of drug administration and the anti-inflammation study. (B) Symptoms of ocular inflammation such as conjunctiva congestion, swelling, and iris hyperemia were examined after each administration group. (C) Conjunctiva scores after each administration group (mean ± SD, $n = 6$). (D) Concentration of PGE_2 in tears after each administration group (mean ± SD, $n = 6$). (E) Histopathology analysis of conjunctiva tissues. Scale bars = 50 μm. (F) Ocular irritation test (mean ± SD, $n = 3$). **$P < 0.01$ and ***$P < 0.001$.

contrast, the FBNa group exhibited mild eye irritation, likely attributable to the presence of the carboxyl group in the FB structure. Conversely, in the S-FBTMA group, TMA partially shielded the exposed carboxyl group through the formation of an ion pair with S-FB, resulting in the absence of any noticeable eye discomfort. Consequently, the safety profile of S-FBTMA was affirmed, suggesting its potential suitability for clinical investigation and use.

4. Conclusion

In summary, our investigation successfully isolated and synthesized R/S-FBNa and analogous salts (S-FBTMA, S-FBDEA and S-FBARG). *In vivo* assessments unveiled no notable stereoselectivity or configurational conversion between R-FB and S-FB. Among the synthesized salts, S-FBTMA exhibited heightened solubility and lipid affinity, suggesting improved corneal permeability. *In vitro* corneal permeation studies confirmed its superior performance. Pharmacokinetic evaluations indicated elevated C_{max} and AUC values for S-FBTMA in aqueous humor and iris. Anti-inflammatory assessments demonstrated S-FBTMA's superior efficacy in reducing ocular inflammation and PGE_2 levels. Histological evaluations illustrated enhanced conjunctival tissue integrity with S-FBTMA. Importantly, S-FBTMA exhibited no eye irritation. These findings propose that S-FBTMA holds promise as a prospective candidate for further preclinical and clinical development in ocular drug delivery.

Conflicts of interest

The authors declare no competing financial interest.

Acknowledgments

This work was financially supported by the National Postdoctoral Foundation of China (No. 2023M730375), Liaoning Province Department of Education Project (No. LJKMZ20221365), and the State Key Laboratory of Natural and Biomimetic Drugs (No. K202215).

Supplementary materials

Supplementary material associated with this article can be found, in the online version, at doi:10.1016/j.ajps.2024.100928.

References

[1] Cantarella RDA, De Oliveira JK, Dorbandt DM, Montiani-Ferreira F. Effects of topical flurbiprofen sodium, diclofenac sodium, ketorolac tromethamine and benzalkonium chloride on corneal sensitivity in normal dogs. Open Vet J 2017;7(3):254–60.
[2] Han S, Shen JQ, Gan Y, Geng HM, Zhang XX, Zhu CL, et al. Novel vehicle based on cubosomes for ophthalmic delivery of flurbiprofen with low irritancy and high bioavailability. Acta Pharmacol Sin 2010;31(8):990–8.
[3] Weng YH, Ma XW, Che J, Li C, Liu J, Chen SZ, et al. Nanomicelle-assisted targeted ocular delivery with enhanced antiinflammatory efficacy *in vivo*. Adv Sci (Weinh) 2018;5(1):1700455.
[4] Mesquida M, Drawnel F, Fauser S. The role of inflammation in diabetic eye disease. Semin Immunopathol 2019;41(4):427–45.
[5] Kandarakis SA, Petrou P, Papakonstantinou E, Spiropoulos D, Rapanou A, Georgalas I. Ocular nonsteroidal inflammatory drugs: where do we stand today? Cutan Ocul Toxicol 2020;39(3):200–12.
[6] Al-Lawati H, Binkhathlan Z, Lavasanifar A. Nanomedicine for the effective and safe delivery of non-steroidal anti-inflammatory drugs: a review of preclinical research. Eur J Pharm Biopharm 2019;142:179–94.
[7] Rodrigues EB, Farah ME, Bottos JM, Bom Aggio F. Nonsteroidal anti-inflammatory drugs in the treatment of retinal diseases. Dev Ophthalmol 2016;55:212–20.
[8] Wilson DJ, Schutte SM, Abel SR. Comparing the efficacy of ophthalmic NSAIDs in common indications: a literature review to support cost-effective prescribing. Ann Pharmacother 2015;49(6):727–34.
[9] El-Sayed MM, Hussein AK, Sarhan HA, Mansour HF. Flurbiprofen-loaded niosomes-in-gel system improves the ocular bioavailability of flurbiprofen in the aqueous humor. Drug Dev Ind Pharm 2017;43(6):902–10.
[10] Yataba I, Otsuka N, Matsushita I, Kamezawa M, Yamada I, Sasaki S, et al. Plasma pharmacokinetics and synovial concentrations of S-flurbiprofen plaster in humans. Eur J Clin Pharmacol 2016;72(1):53–9.
[11] Radwan MA, Aboul-Enein HY. *In vitro* release and stereoselective disposition of flurbiprofen loaded to poly(D,L-lactide- co-glycolide) nanoparticles in rats. Chirality 2004;16(2):119–25.
[12] Uwai Y, Matsumoto M, Kawasaki T, Nabekura T. Enantioselective effect of flurbiprofen on lithium disposition in rats. Pharmacology 2017;99(5–6):236–9.
[13] Zhou X, Wang HS, Zeng Q. Chiral separation of DL-glutamic acid by ultrasonic field. Crystengcomm 2016;19(5):762–6.
[14] Báthori NB, Jacobs A, Mei M, Nassimbeni LR. Resolution of malic acid by (+)-Cinchonine and (-)-Cinchonidine. Can J Chem 2015;93(8):150203143630007.
[15] Ferreira DSP, Ferreira JG, Filho EFS, Princival JL. Tuning lipase-catalysed kinetic resolution of 2-substituted thiophenes and furans: a scalable chemoenzymatic route to masked γ-bis-oxo-alcohols. J Mol Catal B Enzym 2016;126:37–45.
[16] Li M, Guo X, Di X, Jiang Z. Enantioseparation on a new synthetic β-cyclodextrin chemically bonded chiral stationary phase and molecular docking study. Anal Bioanal Chem 2021;413(15):3933–44.
[17] Guggilla S, Karthik M, Shylendra B. Sensitive and stereospecific high-performance liquid chromatographic method for flurbiprofen in human plasma. Adv Exp Med Biol 2021;1339:59–63.
[18] Zhang F, He L, Sun W, Cheng YQ, Liu JT, Ren ZQ. Chiral liquid membrane for enantioselective separation of racemic ibuprofen by L-tartaric acid derivatives. Rsc Adv 2015;5(52):41729–35.
[19] Chen Z, Zhang W, Wang L, Fan H, Wan Q, Wu X, et al. Enantioseparation of racemic flurbiprofen by aqueous two-Phase extraction with binary chiral selectors of L-dioctyl tartrate and L-tryptophan. Chirality 2015;27(9):650–7.
[20] Leipold DD, Kantoci D, Murray ED, Quiggle DD, Wechter WJ. Bioinversion of R-flurbiprofen to S-flurbiprofen at various dose levels in rat, mouse, and monkey. Chirality 2004;16(6):379–87.
[21] Soraci AL, Tapia O, Garcia J. Pharmacokinetics and synovial fluid concentrations of flurbiprofen enantiomers in horses: chiral inversion. J Vet Pharmacol Ther 2005;28(1):65–70.
[22] Morrison PWJ, Khutoryanskiy VV. Advances in ophthalmic drug delivery. Ther Deliv 2014;5(12):1297–315.
[23] Mofidfar M, Abdi B, Ahadian S, Mostafavi E, Desai TA, Abbasi F, et al. Drug delivery to the anterior segment of the eye: a review of current and future treatment strategies. Int J Pharm 2021;607:120924.
[24] Zavala J, López Jaime GR, Rodríguez Barrientos CA, Valdez-Garcia J. Corneal endothelium: developmental strategies for regeneration. Eye (Lond) 2013;27(5):579–88.
[25] Singh M, Bharadwaj S, Lee KE, Kang SG. Therapeutic nanoemulsions in ophthalmic drug administration: concept in formulations and characterization techniques for ocular drug delivery. J Control Rel 2020;328:895–916.
[26] Kour J, Kumari N, Sapra B. Ocular prodrugs: attributes and challenges. Asian J Pharm Sci 2021;16(2):175–91.
[27] Baranowski P, Karolewicz B, Gajda M, Pluta J. Ophthalmic drug dosage forms: characterisation and research methods. ScientificWorldJournal 2014;2014:861904.
[28] Ahmed S, Amin MM, Sayed S. Ocular drug delivery: a comprehensive review. AAPS PharmSciTech 2023;24(2):66.
[29] Bachu RD, Chowdhury P, Al-Saedi ZHF, Karla PK, Boddu SHS. Ocular drug delivery barriers-role of nanocarriers in the treatment of anterior segment ocular diseases. Pharmaceutics 2018;10(1):28.
[30] Kang-Mieler JJ, Dosmar E, Liu W, Mieler WF. Extended ocular drug delivery systems for the anterior and posterior segments: biomaterial options and applications. Expert Opin Drug Deliv 2017;14(5):611–20.
[31] Vedadghavami A, Zhang C, Bajpayee AG. Overcoming negatively charged tissue barriers: drug delivery using cationic peptides and proteins. Nano Today 2020;34:100898.
[32] Otake H, Goto R, Ogata F, Isaka T, Kawasaki N, Kobayakawa S, et al. Fixed-combination eye drops based on fluorometholone nanoparticles and bromfenac/levofloxacin solution improve drug corneal penetration. Int J Nanomed 2021;16:5343–56.
[33] Amrutkar CS, Patil SB. Nanocarriers for ocular drug delivery: recent advances and future opportunities. Indian J Ophthalmol 2023;71(6):2355–66.

[34] Schalnus R. Topical nonsteroidal anti-inflammatory therapy in ophthalmology. Ophthalmologica 2003;217(2):89–98.
[35] Rossy J, Mccanna DJ, Fresco B, Sivak JG. Organ culture system for assessing the toxicity of intraocular treatment excipients and pharmaceuticals. J Vis Exp 2022(179):e63176.
[36] Panfil C, Chauchat L, Guerin C, Rebika H, Sahyoun M, Schrage N. Impact of latanoprost antiglaucoma eyedrops and their excipients on toxicity and healing characteristics in the ex viveo eye irritation test system. Ophthalmol Ther 2023;12(5):2641–55.
[37] Hingorani T, Gul W, Elsohly M, Repka MA, Majumdar S. Effect of ion pairing on *in vitro* transcorneal permeability of a Δ(9) -tetrahydrocannabinol prodrug: potential in glaucoma therapy. J Pharm Sci 2012;101(2):616–26.
[38] Wang T, Zhang Y, Chi M, Zhao C, Cao L, Tian C, et al. A novel fixed-combination timolol-netarsudil-latanoprost ophthalmic solution for the treatment of glaucoma and ocular hypertension. Asian J Pharm Sci 2022;17(6):938–48.
[39] Gaynes BI, Fiscella R. Topical nonsteroidal anti-inflammatory drugs for ophthalmic use: a safety review. Drug Saf 2002;25(4):233–50.
[40] Venardos KM, Rajapakse NW, Williams D, Hoe LS, Peart JN, Kaye DM. Cardio-protective effects of combined L-arginine and insulin: mechanism and therapeutic actions in myocardial ischemia-reperfusion injury. Eur J Pharmacol 2015;769:64–70.
[41] Park H, Seo HJ, Ha ES, Hong SH, Kim JS, Kim MS, et al. Preparation and characterization of glimepiride eutectic mixture with L-arginine for improvement of dissolution rate. Int J Pharm 2020;581:119288.
[42] Cui H, Quan P, Zhou Z, Fang L. Development of a drug-in-adhesive patch combining ion pair and chemical enhancer strategy for transdermal delivery of zaltoprofen: pharmacokinetic, pharmacodynamic and in vitro/in vivo correlation evaluation. Drug Deliv 2016;23(9):3461–70.
[43] Jin Y, Pan Y, Jin B, Jin D, Zhang C. (S)-1-(5-(4-Methylpiperazin-1-yl)-2,4-dinitrophenyl)pyrrolidine-2-carboxylic acid as a derivatization reagent for ultrasensitive detection of amine enantiomers by HPLC-MS/MS and its application to the chiral metabolite analysis of (R)-1-aminoindan in saliva. J Pharm Biomed Anal 2021;194:113815.
[44] Delgado-Perez T, Bouchet LM, De La Guardia M, Galian RE, Perez-Prieto J. Sensing chiral drugs by using CdSe/ZnS nanoparticles capped with N-acetyl-L-cysteine methyl ester. Chemistry (Easton) 2013;19(33):11068–76.
[45] Šupuk E, Ghori MU, Asare-Addo K, Laity PR, Panchmatia PM, Conway BR. The influence of salt formation on electrostatic and compression properties of flurbiprofen salts. Int J Pharm 2013;458(1):118–27.
[46] Bíró T, Horvát G, Budai-Szűcs M, Csányi E, Urbán E, Facskó A, et al. Development of prednisolone-containing eye drop formulations by cyclodextrin complexation and antimicrobial, mucoadhesive biopolymer. Drug Des Dev Ther 2018;12:2529–37.
[47] Shen J, Gan L, Zhu C, Zhang X, Dong Y, Jiang M, et al. Novel NSAIDs ophthalmic formulation: flurbiprofen axetil emulsion with low irritancy and improved anti-inflammation effect. Int J Pharm 2011;412(1–2):115–22.
[48] Fang G, Wang Q, Yang X, Qian Y, Zhang G, Tang B. γ-Cyclodextrin-based polypseudorotaxane hydrogels for ophthalmic delivery of flurbiprofen to treat anterior uveitis. Carbohydr Polym 2022;1(27):118889.
[49] Sou T, Bergström CaS. Automated assays for thermodynamic (equilibrium) solubility determination. Drug Discov Today Technol 2018;27:11–19.
[50] Zhang Q, Wang X, Xue H, Huang B, Lin Z, Cai Z. Determination and comparison of the solubility, oil–water partition coefficient, intestinal absorption, and biliary excretion of carvedilol enantiomers. AAPS PharmSciTech 2021;22(1):43.
[51] Quinteros DA, Tártara LI, Palma SD, Manzo RH, Allemandi DA. Ocular delivery of flurbiprofen based on Eudragit(®) E-flurbiprofen complex dispersed in aqueous solution: preparation, characterization, *in vitro* corneal penetration, and ocular irritation. J Pharm Sci 2014;103(12):3859–68.
[52] Ma R, Qu H, Wang B, Wang F, Yu Y, Yu G. Simultaneous enantiomeric analysis of non-steroidal anti-inflammatory drugs in environment by chiral LC-MS/MS: a pilot study in Beijing, China. Ecotoxicol Environ Saf 2019;174:83–91.
[53] Hanna VS, Hafez EaA. Synopsis of arachidonic acid metabolism: a review. J Adv Res 2018;11:23–32.
[54] Yerramothu P, Vijay AK, Willcox MDP. Inflammasomes, the eye and anti-inflammasome therapy. Eye (Lond) 2017;32(3):491–505.
[55] Wang T, Cao L, Jiang Q, Zhang T. Topical medication therapy for glaucoma and ocular hypertension. Front Pharmacol 2021;12:749858.
[56] Germolec DR, Shipkowski KA, Frawley RP, Evans E. Markers of inflammation. Methods Mol Biol 2018;1803:57–79.
[57] Charmeau-Genevois C, Sarang S, Perea M, Mayer N, Eadsforth C, Austin T, et al. A simplified index to quantify the irritation/corrosion potential of chemicals - Part II: eye. Regul Toxicol Pharmacol 2021;123:104935.
[58] Platania CBM, Fisichella V, Fidilio A, Geraci F, Lazzara F, Leggio GM, et al. Topical ocular delivery of TGF-beta1 to the back of the eye: implications in age-related neurodegenerative diseases. Int J Mol Sci 2017;18(10):2076.
[59] Meyer KaE, Nejad A. CC-stretched formic acid: isomerisation, dimerisation, and carboxylic acid complexation. Phys Chem Chem Phys 2021;23(32):17208–23.
[60] Hachuła B. The nature of hydrogen-bonding interactions in nonsteroidal anti-inflammatory drugs revealed by polarized IR spectroscopy. Spectrochim Acta A Mol Biomol Spectrosc 2018;188:189–96.